[2] Hitt, E. F. and Rea, F. G., "Development of an Evaluation Technique for Strapdown Guidance Systems," Second Interim Scientific Report, Contract NAS 12-550, Feb. 28, 1969, Battelle Memorial Institute, Columbus Labs., Columbus, Ohio.

[3] Rea, F. G. and Fischer, N. H., "An Improved Method of Estimating Midcourse Fuel Requirements (Approximating the Probability Distribution of the Magnitude of a Vector with Normal, Zero Mean, Components)," Paper presented to NASA/ERC Fourth Guidance Theory and Trajectory Analysis Seminar, Cambridge, Mass., May 16–17, 1968.

[4] Strack, W. C. and Huff, V. N., "The N-Body Code, A General FORTRAN Code for the Numerical Solution of Space Mechanics Problems on an IBM 7090 Computer," TN D-1730, Nov. 1963, NASA.

[5] "Saturn IB Improvement Study (Solid First Stage) Phase II, Final Detailed Report," Rept. SM-51896, Vol. II, March 30, 1966, Douglas Missile and Space Systems Div., Huntington Beach, Calif.

[6] "Launch Vehicle Estimating Factors," Jan. 1969, NASA.

[7] "A Study of Jupiter Flyby Missions, Final Technical Report," FZM-4625, May 17, 1966, General Dynamics, Fort Worth Div., Fort Worth, Texas.

MARCH 1970 J. SPACECRAFT VOL. 7, NO. 3

Propellant Position Control by Capillary Barriers during Spacecraft Rotational Maneuvers

D. F. GLUCK*
North American Rockwell Inc., Downey, Calif.

Capillary barriers, which can provide a propellant positioning and expulsion capability for spacecraft propellant tankage, are used in some applications to create an engine restart compartment. However, pitch maneuvers cause propellant motions and inertial forces that act to draw gas through barrier perforations into the compartment. This is opposed by viscous stresses as well as capillary pressures developed by the barrier. From theory and experiments the dependence of the critical Weber number, We_c (Weber number at incipient gas passage through the barrier) during rotational maneuvers on geometry and fraction open barrier area, O_p, is given graphically. The effect of tank and barrier geometry on We_c is obtained by solving Laplace's equation based on an inviscid model of barrier gas-liquid interface dynamics for an impulsively rotated right cylinder. The effect on We_c of O_p, and thus viscous energy dissipation, was obtained from an experimental program of model tank rotations during aircraft Keplerian trajectories.

Nomenclature

a = tank radius
d = diameter of hole or perforation in capillary barrier
$F(t)$ = function of time in Bernoulli equation
g = acceleration or gravity field
h = height of the barrier above the tank bottom, where volume below barrier is taken as an equivalent right circular cylinder
J_1 = Bessel function of first order and first kind
l = normal distance from center of rotation to barrier
O_p = ratio of hole area to total barrier area
P = pressure; P_G = gas pressure
$\mathbf{q}$ = velocity vector
r = a cylindrical coordinate in inertial frame instantaneously coinciding with tank radial coordinate
R = radius of curvature
s = average height of liquid above capillary barrier
t = time
U = velocity in x direction
V = volume of spherical segment
W = velocity in Z direction
We_c = critical Weber number, value of Weber number at incipient gas passage through barrier
W_R = velocity of liquid through barrier hole relative to tank velocity
$\langle W \rangle_R$ = average value of W_R during growth of interface to maximum size
W_t = tank velocity in Z direction
x = coordinate in inertial framework
X = height of spherical segment
Z = coordinate in inertial frame instantaneously coinciding with the tank axis, taken as positive in the downward direction
η = coefficient of bubble pressure term
$\dot{\theta}$ = rotation rate about axis perpendicular to tank longitudinal axis
ν = kinematic viscosity
ξ_n = roots of J_1 (arg) = 0
ρ = liquid density
σ = liquid surface tension
φ = angular coordinate in inertial framework instantaneously coinciding with tank coordinate
Φ = velocity potential
Φ_F = final velocity potential for case of O_p approaching 1
Φ_0 = initial velocity potential for case of O_p approaching 1

Presented as Paper 69-529 at the AIAA 5th Propulsion Joint Specialist Conference, U.S. Air Force Academy, Colo., June 9–13, 1969; submitted June 9, 1969; revision received October 27, 1969.

* Member of the Technical Staff.

Introduction

CAPILLARY barrier devices can provide a propellant positioning and expulsion capability, as well as appreciable slosh dampening, for spacecraft propulsion systems. Such devices, which are sometimes simply perforated plates, function both by utilizing propellant surface tension to generate motion-inhibiting capillary pressures and by providing a mechanism for viscous energy dissipation. The configuration studied herein is one which might be used in a restartable propulsion system that experiences periods of near weightlessness alternating with periods of propellant orienting engine thrust. Referring to Fig. 1, it is obviously important

to assure that the restart compartment remains gas free. The procedure usually followed is based upon hydrostatics; the perforation size is chosen sufficiently small so that the capillary pressure (often called bubble pressure), $\eta\sigma/d$, is smaller than the pressure head, $\rho g(2a)$, due to the maximum acceleration parallel to the barrier surface. This acceleration is typically due to a lateral maneuver or to spinning the spacecraft (centrifugal acceleration in this case). Here η takes on a maximum value of 4 for a perfectly wetted plate and a sharp-edged perforation, but can be as small as 2 for real propellant-barrier combinations.[1] Negative accelerations are not usually the critical design condition, as each hole then functions as a separate capillary tube and the problem is one of interface stability.[2,3]

However, an adverse acceleration is not the only effect that can dislodge propellant from the restart compartment. Another effect, which appears to be at least as important and to the author's knowledge has not been studied heretofore, is a sudden change in rotation rate or transverse velocity. To illustrate this, consider a spacecraft tank filled somewhat above a capillary barrier (Fig. 2). An angular impulse about the pitch or yaw axis is applied to the spacecraft setting it rotating about the spacecraft center of mass. Schematic A depicts a quiescent zero g configuration before the impulse is applied. Schematic B shows the liquid's condition after impulse termination. The tank then rotates at the angular rate $\dot{\theta}$. The lines shown depict propellant motion with respect to the tank. The extent of liquid motion below the barrier appears to depend upon the unrecovered pressure loss due to flow through the barrier; the pressure loss depends primarily on the fraction open barrier area, O_p. The momentum of this flow tends to (but due to the action of bubble pressure, does not necessarily) pull gas through the barrier as the rotation continues (schematic C). The propellant-barrier interaction resulting from such rotations shall be called here the inertial effect or force.

The sequence of events shown in Fig. 2 is representative of what occurs during spacecraft attitude maneuvers. As these maneuvers are important and often indispensable spacecraft functions, dislocation of propellant due to them is a problem of considerable practical importance. Therefore, theoretical and experimental work is conducted to determine the regimes of stable barrier operation, in terms of the relevant parameters; a barrier is considered stable if under inertial loading it prevents gas passage, and unstable if it permits any gas passage.

Theoretical Results

The theoretical development proceeds from the model shown in Fig. 3a. A cylindrical tank filled to a height h just above a capillary barrier is rotated about an axis perpendicular to the symmetry axis located at an arbitrary distance above the liquid surface. The flow, including that in the vicinity of the capillary barrier, is taken to be incompressible, inviscid, irrotational flow (potential flow). This confines the theory to the limiting case of a barrier with $O_p \to 1$, but does not preclude the barrier from exhibiting bubble pressure.

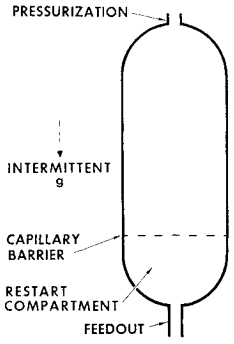

Fig. 1 Design for tanks experiencing a high intermittent gravitational field.

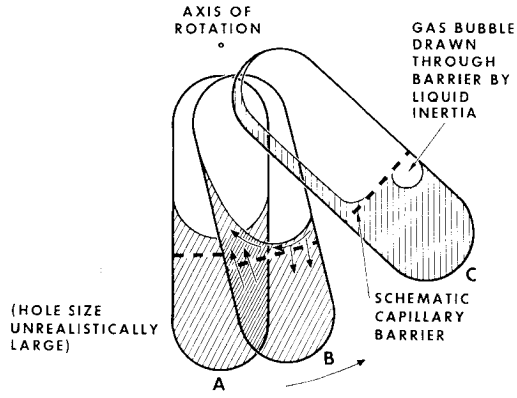

Fig. 2 Propellant dislocation by inertial effect.

A short duration, high-torque angular impulse is applied, instantaneously generating the rotation. The angular velocity, therefore, has step function behavior. The velocity potential satisfies Laplace's equation

$$\nabla^2\Phi = \frac{\partial^2\Phi}{\partial r^2} + \frac{1}{r}\frac{\partial\Phi}{\partial r} + \frac{1}{r^2}\frac{\partial^2\Phi}{\partial\varphi^2} + \frac{\partial^2\Phi}{\partial Z^2} = 0 \qquad (1)$$

where r, φ, and Z are a nonrotating, cylindrical coordinate system with Z positive in the downward direction; $\nabla\Phi = -\mathbf{q}$; and ∇^2 is the Laplacian operator.

The boundary conditions immediately after the impulse is applied are

$$-U_{r=a} = (\partial\Phi/\partial r)_{r=a} = -\dot{\theta}Z\cos\varphi \qquad (2)$$

$$-W_{Z=l+h} = (\partial\Phi/\partial Z)_{Z=l+h} = \dot{\theta}r\cos\varphi \qquad (3)$$

$$\Phi_{Z=l} = 0 \qquad (4)$$

The last condition results from an argument similar to Jacobsen's,[4] as follows. The general form of the Bernoulli equation is

$$-\partial\Phi/\partial t + P/\rho + q^2/2 - gZ = F(t) \qquad (5)$$

Without loss of generality $F(t)$ can be taken equal to zero, and for a delta function impulse the convective and the body force terms can be neglected giving for the impulsive pressure

$$P = \rho(\partial\Phi/\partial t) \qquad (6)$$

If Φ be taken equal to zero at the free surface initially, it follows, since p is zero there throughout the impulse, that immediately after the impulse $\Phi_{Z=l} = 0$.

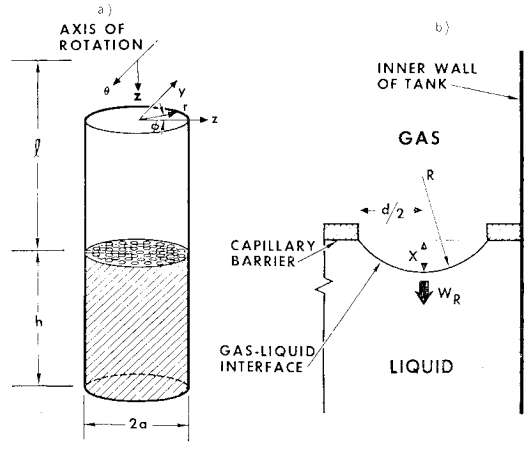

Fig. 3 Model for theoretical development. a) Total model. b) Interface growth at most vulnerable hole.

Solution is obtained to Eqs. (1–4) using separation of variables and following the general methodology of Schmitt[5]

$$\Phi = -\dot{\theta}Zr\cos\varphi + 2\dot{\theta}la\cos\varphi \sum_{n=1}^{\infty} \frac{J_1(\xi_n r/a)\cosh(\xi_n/a)[Z-(l+h)]}{(\xi_n^2-1)J_1(\xi_n)\cosh(\xi_n h/a)} + 4a^2\dot{\theta}\cos\varphi \sum_{n=1}^{\infty} \frac{J_1(\xi_n r/a)\sinh(\xi_n/a)(Z-l)}{\xi_n(\xi_n^2-1)J_1(\xi_n)\cosh(\xi_n h/a)} \quad (7)$$

This tends to cause gas to be drawn through the barrier due to the inertial effect. Considering counterclockwise rotation in Fig. 3a, the tendency for gas passage is strongest for the hole at the extreme right. Therefore, establishing that this hole will not pass gas assures the stability of the entire capillary barrier. Figure 3b shows a blow-up for the right-most portion of the barrier during rotation. Gas passage is counteracted by the bubble pressure associated with the curved gas-liquid interface. A streamline below the right-most hole, as depicted by the arrow in Fig. 3b, is considered.

The liquid pressure can be related to the gas pressure, the curvature, and the surface tension by

$$P = P_G - 2\sigma/R \quad (8)$$

Introducing (8) into (5) and taking $F(t) - P_G/\rho = 0$, there results

$$-\partial\Phi/\partial t - 2\sigma/\rho R + q^2/2 - gZ = 0 \quad (9)$$

As the time after termination of the angular impulse is being considered the convective and body force terms in the Bernoulli equation are not necessarily negligible as was previously the case. However, it is clear that the barrier hole size and, therefore, R, can be made sufficiently small that the term $2\sigma/\rho R$ dominates the terms $q^2/2$ and gZ. Criteria for neglecting these terms have already been developed.[6] Equation (9) upon multiplication by dt now reduces to

$$(\partial\Phi/\partial t)dt + (2\sigma/\rho R)dt = 0 \quad (10)$$

The initially flat interface grows to a hemispherical shape of diameter d through a succession of spherical segments such as shown in Fig. 3b. Defining W_R as the liquid velocity relative to the hole, one can write

$$dt = (4/\pi d^2 W_R)dV \quad (11)$$

Also, V can be written in terms of the segment height X as

$$V = (\pi X/2)[d^2/4 + X^2/3] \quad (12)$$

$$dV = (\pi/2)[d^2/4 + X^2]dX \quad (13)$$

From geometry

$$R = (d^2/4 + X^2)/2X \quad (14)$$

Substituting (11, 13, and 14) into (10)

$$(\partial\Phi/\partial t)dt + (8\sigma/d^2\rho)XdX/W_R = 0 \quad (15)$$

The critical case for stability occurs when the interface is pulled just to the hemispherical shape, for then the bubbles being in immediate proximity may coalesce. Thus, the limits of integration of the second term are $X = 0$ and $X = d/2$

$$\int_0^t \frac{\partial\Phi}{\partial t}dt + \frac{8\sigma}{d^2\rho}\int_0^{d/2}\frac{XdX}{W} = 0 \quad (16)$$

The velocity W_R is an undetermined function of X; however, the equation can be integrated if some type of mean velocity $\langle W\rangle_R$ is introduced.

The first term in (16) is the change in the potential function at the right-most hole during the growth of the interface to hemispherical shape. This term can be taken as the difference between a final and initial potential;

$$\int_0^t \frac{\partial\Phi}{\partial t}dt = \Phi_F - \Phi_0 \quad (17)$$

The initial potential Φ_0 is given by Eq. (7). It remains to determine the final potential Φ_F for the case of incipient gas passage. In this case, the right-most bubble attains a hemispherical shape, but does not pass through the barrier. As the capillary barrier now blocks gas passage, it is hypothesized here that the final potential Φ_F can be approximated by that which would occur if the barrier were replaced by a solid lid. The boundary conditions are now

$$-U_{r=a} = (\partial\Phi/\partial r)_{r=a} = -\dot{\theta}Z\cos\varphi \quad (18)$$

$$-W_{Z=l+h} = (\partial\Phi/\partial Z)_{Z=l+h} = \dot{\theta}r\cos\varphi \quad (19)$$

$$-W_{Z=l} = (\partial\Phi/\partial Z)_{Z=l} = \dot{\theta}r\cos\varphi \quad (20)$$

The solution to Laplace's equation subject to (18–20) is

$$\Phi = \dot{\theta}Zr\cos\varphi + 4a^2\dot{\theta}\cos\varphi \sum_{n=1}^{\infty} \frac{J_1(\xi_n r/a)\sinh(\xi_n/a)[Z-(l+h/2)]}{\xi_n(\xi_n^2-1)J_1(\xi_n)\cosh(\xi_n h/2a)} \quad (21)$$

What has been hypothesized, then, is that during the rotation, the action of bubble pressure has shut off the flow through the barrier converting the flowfield from Φ_0 [Eq. (7)] to Φ_F [Eq. (21)]. The flowfield Φ_F is, of course, not the exact solution since: 1) the tank has rotated through some small angle before flow through the barrier has halted, whereas Φ_F is the $\theta = 0$ flowfield; 2) the action of bubble pressure is not expected to be identical to that of a solid lid. However, it is believed that Φ_F of Eq. (20) is a good estimate of the flowfield for the case of incipient gas passage.

Equation (16) is therefore integrated to give

$$\Phi_F - \Phi_0 + \sigma/\rho\langle W\rangle_R = 0 \quad (22)$$

where Φ_F and Φ_0 are to be evaluated at the right-most barrier hole. From Eq. (21)

$$(\Phi_F)_{Z=l,\ r=a,\ \varphi=0} = -la\dot{\theta} - 4a^2\dot{\theta}\Sigma_1 \quad (23)$$

where

$$\Sigma_1 = \sum_{n=1}^{\infty} \tanh\left(\frac{\xi_n h}{2a}\right)\Big/\xi_n(\xi_n^2-1)$$

From Eq. (7)

$$(\Phi_0)_{Z=l,\ r=a,\ \varphi=0} = 0 \quad (24)$$

Differentiating Eq. (7)

$$W = -\frac{\partial\Phi}{\partial Z} = -\dot{\theta}r\cos\varphi + 2\dot{\theta}l\cos\varphi \sum_{n=1}^{\infty} \frac{\xi_n J_1(\xi_n r/a)\sinh(\xi_n/a)[Z-(l+h)]}{(\xi_n^2-1)J_1(\xi_n)\cosh(\xi_n h/a)} + 4a\dot{\theta}\cos\varphi \sum_{n=1}^{\infty} \frac{J_1(\xi_n r/a)\cosh(\xi_n/a)(Z-l)}{(\xi_n^2-1)J_1(\xi_n)\cosh(\xi_n h/a)} \quad (25)$$

and

$$W_{Z=l,\ r=a,\ \varphi=0} = a\dot{\theta} + 2l\dot{\theta}\Sigma_2 - 4a\dot{\theta}\Sigma_3 \quad (26)$$

where

$$\Sigma_2 = \sum_{n=1}^{\infty} \xi_n \tanh\left(\frac{\xi_n h}{a}\right)\Big/(\xi_n^2-1)$$

$$\Sigma_3 = \sum_{n=1}^{\infty} 1\Big/\left[(\xi_n^2-1)\cosh\left(\frac{\xi_n h}{a}\right)\right]$$

and the positive direction of W is defined as downward (the reverse of the usual definition).

To determine the relative velocity of the liquid the tank velocity, W_t, must be subtracted from W

$$(W_l)_{Z=l,\ r=a,\ \varphi=0} = -a\dot{\theta} \tag{27}$$

Therefore

$$(W_R)_{Z=l,\ r=a,\ \varphi=0} = 2a\dot{\theta} + 2l\dot{\theta}\Sigma_2 - 4a\dot{\theta}\Sigma_3 \tag{28}$$

For the critical case of incipient gas passage through the barrier, W_R varies from the value given in Eq. (28) to zero. Considering the approximations already made, it is reasonable to take $\langle W\rangle_R$ as $W_R/2$. Doing this, and substituting (23, 24, and 28) into (22), and rearranging, an equation for the critical Weber number at incipient gas passage through the barrier is obtained

$$We_c = (\dot{\theta}^2 a^3\rho/\sigma)_c = \{(l/a + \Sigma_1)[1 + (l/a)\Sigma_2 - 2\Sigma_3]\}^{-1} \tag{29}$$

A difficulty yet remains; the second series, Σ_2 in (29) is not convergent. This is readily explained, as the potential solution for a step function rotation rate gives a circle of singularity at $Z = l$, $r = a$. Thus, the velocities given by Eqs. (26) and (28) blow up at $Z = l$, $r = a$. It is clear that in reality, this difficulty is removed as the liquid is not inviscid, and in fact, the appropriate boundary condition at the wall

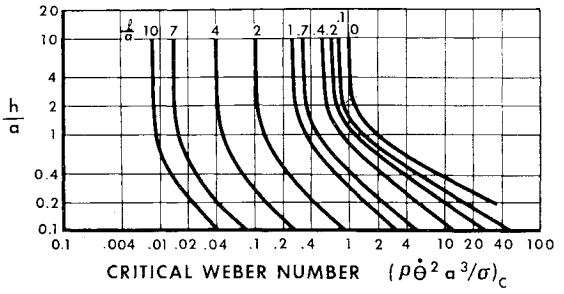

Fig. 4 Critical Weber number as a function of geometry and position of axis of rotation.

[in addition to (2)] is that $W_R = 0$. Furthermore, a small distance from the wall, potential flow assumptions hold. This suggests evaluating the terms in Eq. (22) at some small distance from the wall. However, this complexity does not appear warranted considering the idealization of the theoretical model. Therefore, the second term in Eq. (26) has been evaluated at

$$Z = l + a(1 - r/a),\ r = a(r/a),\ \varphi = 0$$

Velocities were determined at various values of r/a near 1 and it was found that below values of $r/a = 0.95$ the relative velocity and, therefore, We_c changed slowly with r/a. Thus Σ_2 is evaluated at $Z = l + 0.05a$, $r = 0.95a$, Eq. (29) changing accordingly as given below

$$We_c = \left(\left\{\frac{l}{a} + 4\Sigma_1\right\}\left\{1 + \frac{l}{a}\sum_{n=1}^{\infty}\left[\frac{\xi_n J_1(0.95\xi_n)}{(\xi_n^2 - 1)J_1(\xi_n)}\right]\times \left[\tanh\left(\frac{\xi_n h}{a}\right)\cosh(0.05\xi_n) - \sinh(0.05\xi_n)\right] - 2\Sigma_2\right\}\right)^{-1} \tag{30}$$

This is the sought-for result relating the conditions at incipient gas passage through the barrier to the tank geometry and location of the axis of rotation for the limiting case of a perfectly open barrier. It is noteworthy that the barrier hole size d does not enter into this relationship. This result is in marked contrast to those for the stability of a barrier in an acceleration field as has been discussed earlier.

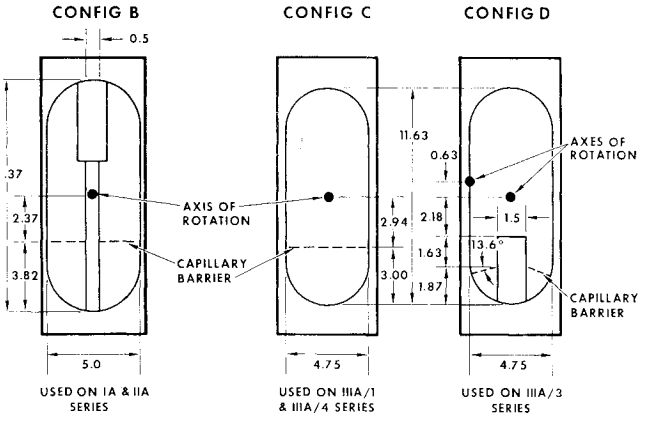

Fig. 5 Test models.

Using Eq. (30), critical Weber numbers were calculated on an IBM 7090 for a range of h/a and l/a. Results are presented in Fig. 4. This figure shows that We_c decreases with increasing l/a and h/a over the whole range of l/a and up to values of h/a of about 2.5; it becomes essentially independent of h/a when $(h/a) > 2.5$.

Experimental Program

The main limitation of this theory is the requirement of an openness ratio of 1. Although there are some practical cases when a barrier with O_p near 1 may be used, it is more often the case that O_p is below 0.5. For these cases We_c is expected to be a strong function of O_p, as well as the geometric groups h/a and l/a. To determine this dependence an extensive experimental program was conducted. This program is described in detail in Ref. 6, and in abbreviated form in what follows.

The tests were conducted using 4.75 and 5.00-in. i.d. plexiglas model tanks, so designed that any one of several capillary barrier configurations could be installed for a given test. The models used are shown in Fig. 5. Carbon tetrachloride was the test fluid. Tests were conducted in a 2 ft × 2 ft × 4 ft test package containing a rotating mechanism, timer, lights, and camera (Fig. 6). The design of the rotating mechanism was such that the axis of rotation could be located at various positions with respect to the tank model.

The test facility was the Boeing KC-135 flying laboratory operating out of Patterson Field at Wright-Patterson Air Force Base, Dayton, Ohio. This aircraft flies a parabolic, that is Keplerian, trajectory, which permits the tests to be conducted in a near weightless environment. Twenty-two of the tests, constituting one-half of the total conducted, proved suitable for quantitative analysis. A test was re-

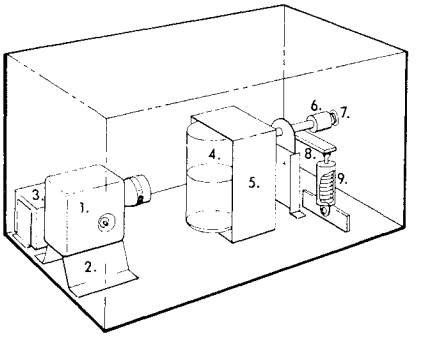

Fig. 6 Test package schematic. 1—Camera, 2—camera mount, 3—timer, 4—tank model, 5—tank mounting bracket and light box, 6—magnetic brake, 7—clutch, 8—rotating shaft arm, 9—return spring assembly.

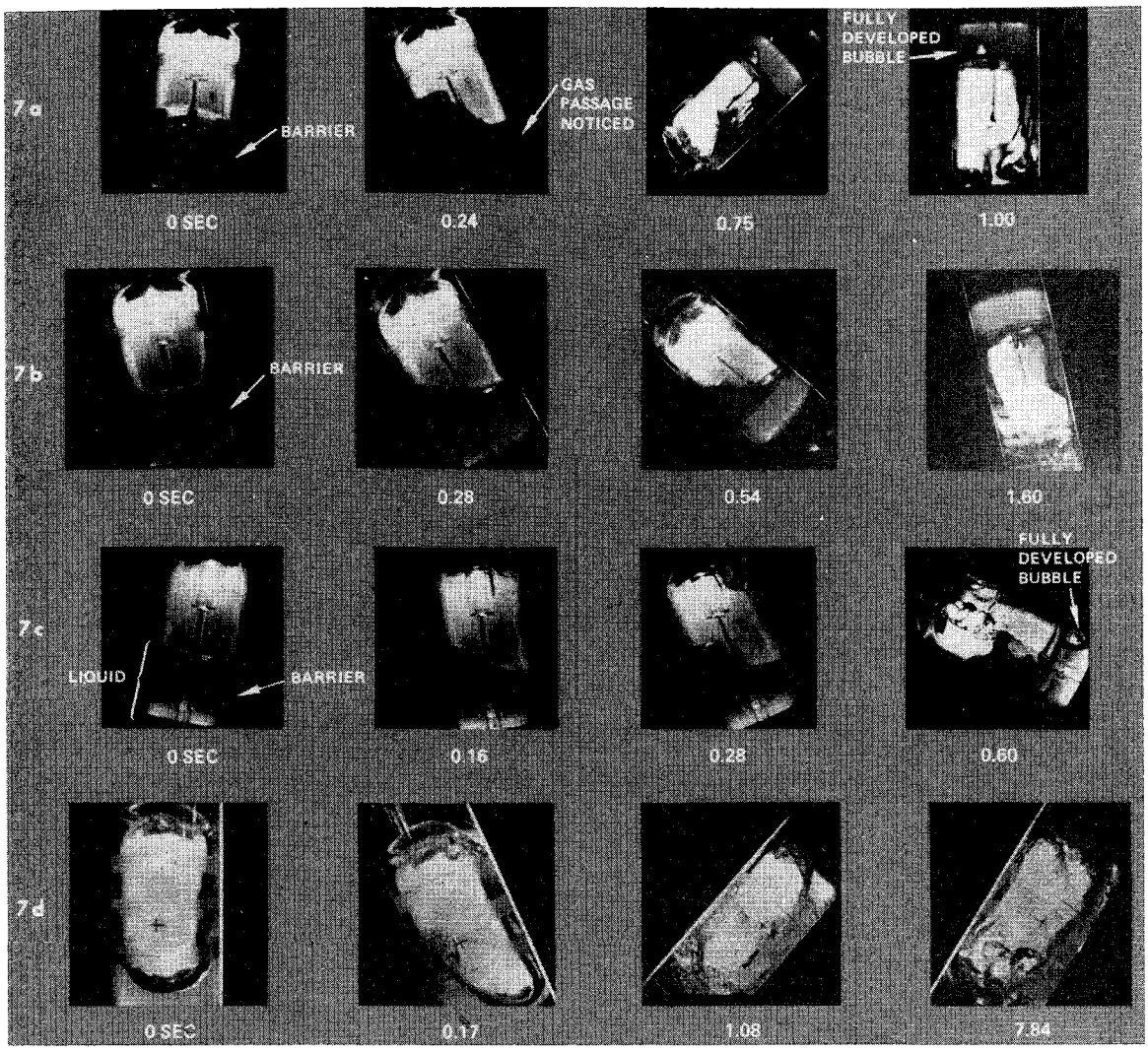

Fig. 7 Representative tests.

jected if 1) the liquid was not essentially quiescent before the rotation of the tank, 2) the tank was still being accelerated by the rotation mechanism when the barrier was exposed to gas, or 3) the test package was jolted or jarred before the test was completed. The test film data was reduced using a Model 29E Telereadex-Telecordex Film Reader, manufactured by the Benson-Lehner Corporation. From tank position vs time data, tank angular velocities and accelerations were determined; the angular velocities were used to determine the test Weber number.

Experimental Results

Photographs from four representative tests are shown in Fig. 7. The test conditions are given in Table 1. Four frames from run 11A/3-12 are shown in Fig. 7a. Time zero corresponds to the beginning of the rotation. Gas, which passes through the barrier due to the inertia effect, can be seen below the barrier by 0.24 sec. This test, therefore, is an example of unstable barrier action. When the rotation is halted (not shown) the bubble detaches from the barrier and lodges in the barrier compartment.

Table 1 Representative tests

Fig.	Run	Config.	Barrier hole size	Barrier fraction open area	Rotation rate, rad/sec
7a	IIA/3-12	B	0.050 in.	0.30	4.0
7b	IIA/3-13	B	0.050 in.	0.30	1.45
7c	IA/1-3	B	0.040 in.	0.46	2.33
7d	IIIA/5-8	C	No barrier		2.20

Run 11A/3-13 (Fig. 7b) differs from 11A/3-12 in having a lower rotation rate, 1.45 in contrast to 4.00 rad/sec. This lower rate is not sufficient to draw gas through the barrier. Scrutiny of the data film shows that the barrier is exposed to some gas by 0.40 sec, and by 0.54 sec, about a third of the barrier's upper surface is dry. This test is an example of stable barrier operation.

Run 1A/1-3 (Fig. 7c) is another example of unstable barrier operation. Gas begins to pass through the barrier at 0.16 sec. The bubble size is greater than that of Run 11A/3-12, despite a lower rotation rate. This is due to a larger fraction open area of this barrier ($O_p = 0.46$ compared to $O_p = 0.30$). It will be seen shortly that not only does O_p affect the bubble size, but it has an important influence on the stability of the barrier. The barrier used in this test is seen as a thin dark line. Tape used to seal the model on the outside prevents direct viewing of the barrier, and this tape is seen as a gray band.

In Run 111A/5-8 (Fig. 7d), no barrier was used. The initial conditions were not perfect; some liquid can be seen on the right wall at time zero. However, the liquid motion due to the rotation is typical of the tests with no capillary barrier. From 0.17 to 0.70 sec, the tank "bottom" is largely depleted of liquid. Termination of the rotation, at about

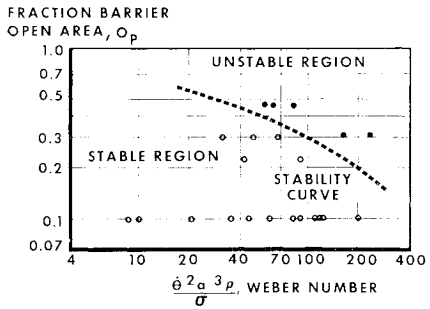

Fig. 8 Capillary barrier stability results.

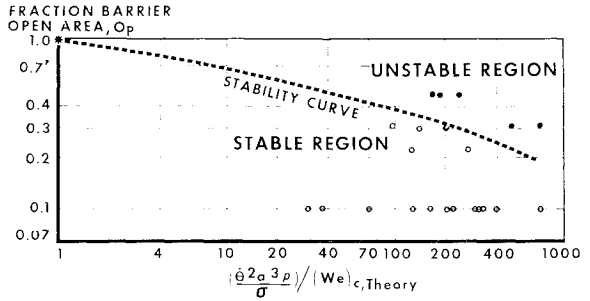

Fig. 9 Normalized capillary barrier stability results.

1.5 sec, transfers the liquid momentum generated by the rotation of the tank into the energetic, bubbly, random motion seen thereafter. This test serves to demonstrate by comparison with the others that capillary barriers act not only to position propellant but also as slosh baffles.

Of the twenty-two useful test runs, the barrier functioned stably in seventeen and unstably in five. For reference, the test parameters and dimensionless groups are given in tabular form in Ref. 6. Because O_p appeared to greatly affect screen stability, the results are presented in Fig. 8 as O_p against We. The unstable points are plotted as solid circles; stable points, as open circles. The data obtained for $O_p = 0.1$ are well within the region of stable operation. Tests at $O_p = 0.22$, 0.30, and 0.46 fall in the stable and unstable regions and define, at least roughly, a stability curve. The region above this curve is called the stable region and that below the unstable region.

It would be very surprising if two variables alone would define the stability characteristics of the barrier. Simple dimensional considerations indicate a relationship at least as complicated as

$$\text{Stability} = \text{Func.}(O_p, \dot{\theta}^2 a^3 \rho/\sigma,\ l/a,\ h/a,\ d/a,\ s/a, \dot{\theta} a d/\nu)$$

No quantitative results of the effect of groups s/a, $\dot{\theta}ad/\nu$ (a form of Reynolds number), and d/a were obtained. However, the qualitative trends seem discernable. It was evident from the test photos that the more liquid initially above the barrier (large s) the more stable the barrier. The tests were made with s/a varying from 0.25 to 1.0, which is probably a realistic range for actual spacecraft operation. It is believed that the stability results obtained for these tests are essentially independent of Reynolds number. This is founded on the belief that the significant Reynolds number is that which is based on the barrier hole size—as the contraction coefficient, and, therefore, the unrecovered pressure loss for flow through the barrier holes is a function of this Reynolds number. However, the dependence of the contraction coefficient on Reynolds number is weak—the unrecovered pressure loss being a much stronger function of O_p. Finally, the theoretical results indicated that the effect of d/a on barrier stability is small, especially if $(d/a) \ll 1$.

The groups l/a and h/a have already been encountered in determining the critical Weber number for $O_p = 1$ [Eq. (30)]. It is proposed here that the same form of solution can be used to account for l/a and h/a for all values of O_p. Therefore, the results are presented in Fig. 9 as a plot of O_p against the test Weber number divided by the Weber number calculated from Eq. (30). This form of presentation allows inclusion of a theoretical data point (represented by an asterisk) at $O_p = 1$. A stability curve was drawn from the theoretical point through the experimental data. To the author's knowledge, no other design criterion exists for the stability of capillary barriers under inertial loads due to rotations, and therefore, this curve is recommended for appropriate design purposes.

References

[1] Gille, J. P. and Zukoski, E. E., "Capillary Barrier Technology," Rept. SD 67-1217, 1967, Space Div., North American Rockwell, Downey, Calif.

[2] Bretherton, F. P., "The Motion of Long Bubbles in Tubes," *Journal of Fluid Mechanics*, Vol. 10, 1961, pp. 166–188.

[3] Gluck, D. F. and Gille, J. P., "Fluid Mechanics of Zero-g Propellant Transfer in Spacecraft Propulsion Systems," *Transactions of the ASME, Ser. B*, Vol. 87, No. 1, Feb. 1965, pp. 1–8.

[4] Jacobsen, Lydik S., "Impulsive Hydrodynamics of Fluid Inside a Cylindrical Tank and of Fluid Surrounding a Cylindrical Pier," *Bulletin of the Seismological Society*, Vol. 39, 1949, pp. 189–204.

[5] Schmitt, A. F., "Forced Oscillations of a Fluid in a Cylindrical Tank," Rept. ZU-7-069, 1956, Convair Div., General Dynamics, San Diego, Calif.

[6] Gluck, D. F., Lofland, M. L., and Gille, J. P., "Hydrodynamic Stability of Capillary Barriers for Spacecraft Propellant Position Control," Rept. SID 66-1087, 1966, North American Rockwell, Space Div., Downey, Calif.